atmosphere

MDPI

Communication

Two Decades of Satellite Observations of Carbon Monoxide Confirm the Increase in Northern Hemispheric Wildfires

Leonid Yurganov [1,*] and Vadim Rakitin [2]

[1] Joint Center for Earth Systems Technology, University of Maryland Baltimore County, Baltimore, MD 21250, USA
[2] Laboratory of Atmospheric Spectroscopy, A.M. Obukhov Institute of Atmospheric Physics, Russian Academy of Sciences, Moscow 119017, Russia
* Correspondence: leonid.yurganov@gmail.com

Abstract: Biomass burning is an important and changing component of global and hemispheric carbon cycles. Boreal forest fires in Russia and Canada are significant sources of the greenhouse gases carbon dioxide (CO_2) and methane (CH_4). The influence of carbon monoxide (CO) on the greenhouse effect is practically absent; its main absorption bands of 4.6 and 2.3 μm are far away from the climatically important spectral regions. Meanwhile, CO concentrations in fire plumes are closely related to CO_2 and CH_4 emissions from fires. On the other hand, satellite measurements of CO are much simpler than those of the aforementioned gases. The Atmospheric Infrared Sounder (AIRS) operating in the Thermal IR spectral region has provided a satellite-based CO data set since October 2002. This satellite data allow to estimate CO emissions from biomass burning north of 30° N using a simple two-box mass-balance model. These results correlate closely with independently estimated CO emissions from the GFED4c bottom-up database. In 2021, both estimate record high emissions throughout the preceding two decades, double the annual emissions compared to previous periods. There have been two years with extremely high emissions (2003 and 2021) but for the rest of the data, an upward trend with a rate of 3.6 ± 2.2 Tg CO yr^{-2} ($4.8 \pm 2.7\%$ yr^{-1}) was found. A similar rate of CO emissions can be seen in the GFED4c data.

Keywords: thermal infrared satellite data; carbon monoxide; boreal fires; carbon dioxide

Citation: Yurganov, L.; Rakitin, V. Two Decades of Satellite Observations of Carbon Monoxide Confirm the Increase in Northern Hemispheric Wildfires. *Atmosphere* **2022**, *13*, 1479. https://doi.org/10.3390/atmos13091479

Academic Editor: Yusheng Shi

Received: 19 August 2022
Accepted: 8 September 2022
Published: 12 September 2022

1. Introduction

Boreal forest fires (wildfires) in the Northern Hemisphere have various impacts on the environment and the climate system. Changes in evapotranspiration, the surface heat regime, productivity, soil respiration, and post-fire changes in albedo on the burned areas, are just some examples of adverse climatic effects [1]. Emissions of greenhouse gases are included in these unacceptable phenomena. Estimating the amount of greenhouse gases emitted by natural fires is not simple. A so-called "bottom-up" approach is based on burned areas and assimilates data on dry organic matter per unit of burned area, emission factors for specific gases, and types of burning and/or smoldering [2]. Many parameters in these calculations are not accurately known. In particular, Siberian fires are the most difficult due to the extremely rare ground network of observation points. Nevertheless, significant progress has been achieved in the use of this technique [3,4].

In another approach called the "top-down" or "inversion" approach, greenhouse gas (GHG) emissions are derived from measurements of gas concentrations in the atmosphere using various ways: from the ground, from aircraft, or from satellite. The advantage of satellite concentration measurements over others is their global coverage. The main disadvantage of satellite Thermal IR (TIR) methods is their low accuracy for the planetary boundary layer that is primarily polluted by fires. Therefore, they need to be corrected for lower sensitivity by comparing to more accurate ground-based spectroscopic solar tracking measurements. Validation is necessary, but in any case, the current validation network is

not dense enough. Nevertheless, the combination of top-down and bottom-up approaches to the study of greenhouse gas emissions seems promising.

Carbon monoxide (CO) is the second most common product of wildfires after carbon dioxide (CO_2). Its background concentration is ~4000 times less than that of CO_2. The strong CO fundamental absorption band near the 4.6 μm wavelength is just slightly overlapped by water vapor (H_2O) lines. Therefore, this species has been a widely recognized proxy for wildfires and urban emissions [5,6]. The two longest satellite CO TIR data sets are presently available. The Measurement of Pollution in The Troposphere (MOPITT, 2000–now) [7] and Atmospheric Infrared Sounder (AIRS, 2002–now) [8] provide total columns (TC) and profiles globally. Yearly CO fluctuations in summer have been caused by biomass burning [6,9,10]. Annual concentrations of carbon monoxide have been decreasing since 2000 [11]. The decline is particularly noticeable in the Northern Hemisphere. This is caused by technological and regulatory innovations in transport and industry [11].

The first attempt to estimate CO emissions from fires in 2002–2003 based on satellite data in combination with ground-based sampling in the High Northern Hemisphere (HNH, 30° N–90° N) was undertaken based on the mass-balance model [9]. Previously, this model was developed to study the boreal fires of 1998 [10]. An alternative to the box model is the global three-dimensional chemical transport model (CTM). Such a model has been applied to the MOPITT dataset for 2000–2017 [11] and inferred surface fluxes of CO from many sources, with a spatial resolution of 3.75° longitude × 1.9° latitude. Global wildfires in 2000–2019 were also investigated by [12].

In this report, we estimated all CO emissions from HNH fires from 2002 to 2021 using AIRS data and the box model described in previous publications [9,10]. The necessary parameters of the model (photochemical removal rate, air exchange between the tropical and extratropical northern hemisphere, etc.) were unchanged from the previous results. A comparison with the independent estimates of the Global Fire Emission Database (GFED4c) [3] showed reasonable random differences between the monthly data sets of less than ±10 Tg CO mon^{-1} for most of the data except for a few points. Both the bottom-up GFED4c method and the top-down AIRS method clearly show an upward trend in forest fire emissions over the past 20 years.

2. Materials and Methods

2.1. AIRS Data and Validation

AIRS is a diffraction grating spectrometer that was launched in a sun-synchronous polar orbit in May 2002 on board the Aqua satellite [8]. The instrument scans ±48.3° from the nadir, which provides almost full global daily coverage. The spectral resolution is 1.79 cm^{-1} at the CO fundamental absorption band near the 4.6 μm wavelength. The instrument has a 13.5 km spatial resolution at the nadir. Currently (September 2022), the AIRS is still operational. A new version 7 of the data [13] is characterized by improved consistency between day and night water vapor; improved temperature products; improved AIRS IRonly retrievals, especially in the high latitude regions; and the removal of ambiguity in surface classifications in the infrared-only (IR-only) retrieval algorithm. Monthly and daily average data (Level 3) between October 2002 and July 2022 for ascending and descending orbits are available online in a 1° × 1° latitude/longitude grid at https://disc.gsfc.nasa.gov/datasets/ (accessed on 10 August 2022), AIRS3STM_7.0 (monthly) and AIRS3STD_7.0. (daily). Reduced sensitivity of AIRS CO to the lower troposphere required a correction coefficient (see Section 3.1).

The chosen box model deals with the monthly total amounts of gas in the box. For our needs, we averaged the CO for ascending orbits in molec cm^{-2} (or the vertically averaged volume mixing ratio Xco in ppb) over the HNH. After that, it was multiplied by the area of the box to obtain the total amount of CO in Tg.

All satellite data needed to be verified. Xco are regularly measured by the Total Carbon Column Observing Network (TCCON) [14] from the spectrally resolved infrared solar radiation recorded by the Bruker IFS 125HR instruments. These Michelson-type Fourier transform IR (FTIR) interferometers with solar tracking and a resolution of ~0.02 cm^{-1}

operate in the first overtone absorption band near 2.3 μm. The Zvenigorod scientific station of the Obukhov Institute of Atmospheric Physics is equipped with a diffraction grating solar tracking spectrometer with a spectral resolution of about 0.2 cm^{-1} [15] covering the main CO band of about 4.6 μm. AIRS L3 daily averages for the 1° × 1° latitude/longitude grid cells coinciding with nine test points (Table 1) were compared with the Xco determined from the ground.

Table 1. Validation sites, locations, and parameters of linear regression.

Site	Latitude; Longitude	Slope	Interception	R
E. Trout Lake, Canada	54.35; −104.99	0.82	5.43	0.71
Karlsruhe, Germany	49.1; 8.438	0.74	9.23	0.76
Lamont, OK, USA	36.604; −97.486	0.58	23.25	0.52
Ny-Alesund, Svalbard	78.9; 11.9	0.90	13.01	0.81
Park Falls, PA, USA	45.945; −90.273	0.71	14.41	0.63
Rikubetsu, Japan	43.4567; 143.7661	0.61	26.37	0.61
Sodankyla, Finland	67.3668; 26.631	0.79	9.67	0.86
Tsukuba, Japan	36.0513; 140.1215	0.51	35.38	0.53
Zvenigorod, Russia	55.6957; 36.4454	0.89	−2.64	0.24

2.2. Validation Results

AIRS Xco data were retrieved from the spectrally resolved outgoing thermal IR radiation. The underestimation of TIR satellite CO data was fundamentally conditioned. The AIRS processing algorithm required an a priori profile derived from the pool of available in situ CO profiles [13]. This profile was presumed to have not been perturbed by local sources. The closer the true profile is to the a priori, the higher the accuracy of the remote measurement. Meanwhile, fires and urban pollution affect the lower atmosphere where AIRS sensitivity is reduced.

Ground-based TCCON instruments determined the Xco from the solar radiation spectra; their sensitivity function has a maximum near the surface and only slowly decreases with height. Thus, this network is a reliable verification tool for Xco. All chosen stations are located north of 30° N and in different proximity to the fires.

Figure 1 compares the daily average Xco values measured by the ground-based facilities ("ground truth") and AIRS. The linear least-squares regression parameters are listed in Table 1. We found the overall mean slope of the AIRS regression lines to be 0.73 ppb/ppb with a standard deviation of 0.14 ppb/ppb. The 19% variation in the slopes is due to the different conditions at the validation sites. For example, the city of Tsukuba, where the slope was only 0.53, is located near Tokyo, Japan; it is affected by urban pollution in the lower troposphere.

The physical meaning of the slope is empirical sensitivity, that is the response of the retrieved AIRS Xco to a unit change in the true value. The slope averaged over all nine sites was used to correct for CO variations detected by AIRS. The scatter in slopes for these sites was considered as a measure of the accuracy of the correction factor. Intercepts (Table 1) are not related to sensitivity; the emission rate estimated by the box model was proportional to the monthly change in Xco and not to the concentration itself. For validation, the CO measurements from July–August 2013–2021 were used.

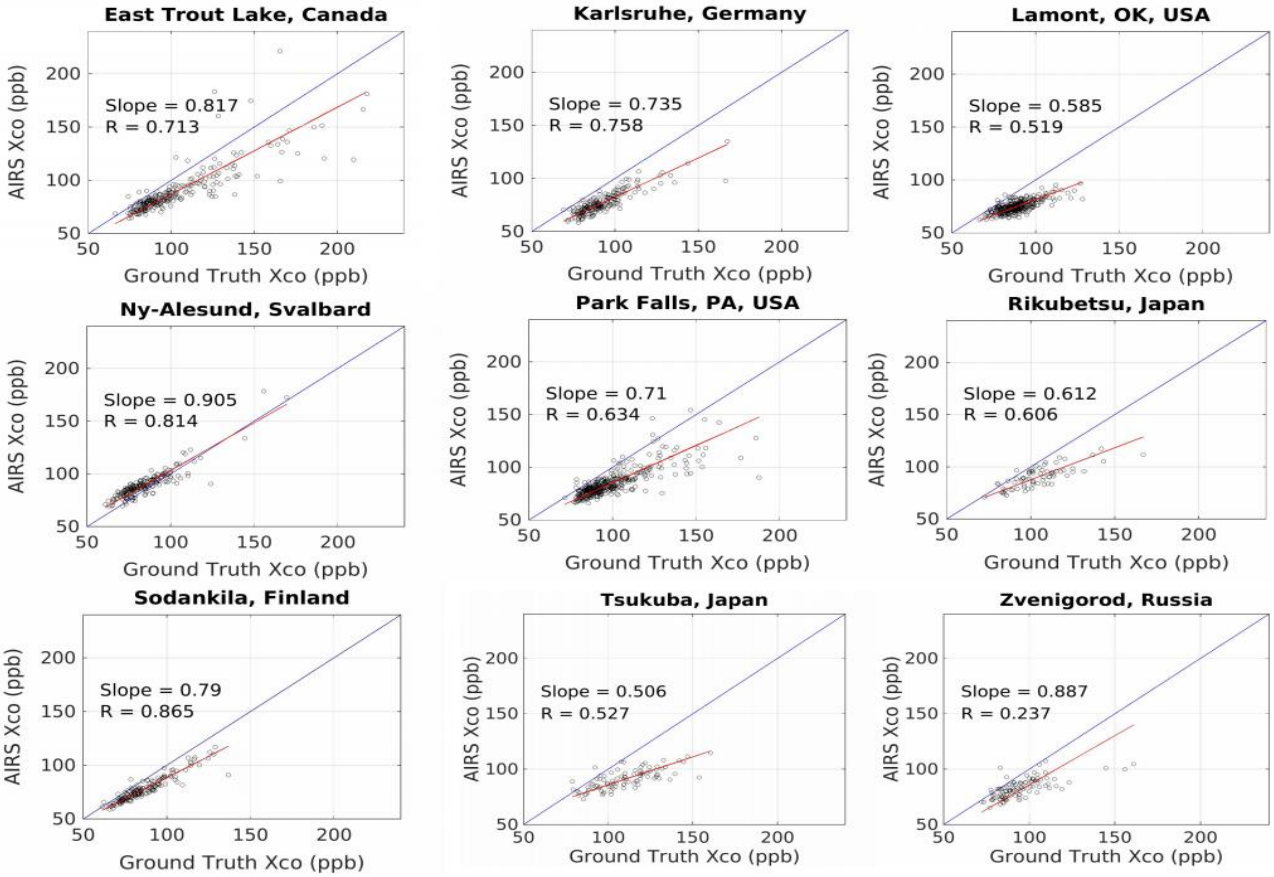

Figure 1. Daily mean Xco measured by AIRS compared with ground-based network.

2.3. Mass-Balance Box Model

A box model is an alternative to a global CTM. It is based on a general idea of a relatively slow exchange of air between the HNH and the Low Northern hemisphere (LNH, 0°–30° N). Wildfires emit CO and this excess CO is relatively quickly spread over the HNH. Leaks to the LNH (transport loss) were estimated from an available CTM model [10,16] (Table A1). A significant part of the pyrogenic CO is oxidized by tropospheric hydroxyl OH (Equation (4)) and was also counted.

The calculation procedure was as follows:

1. Satellite-measured CO volume mixing ratio (VMR) profiles were supplied for 24 standard air layers from the surface to pressure 1.0 hPa with different pressure thicknesses Δp(i) in hPa, where i was from 1 to 24. VMR weighted by Δp(i) averages were calculated for the sake of comparability with the validation network TCCON. The conversion of Xco (ppb) into TC (molec cm^{-2}) was performed as follows: $TC = Xco \cdot 2.12 \cdot 10^{13} \cdot \Sigma(\Delta p(i))$.
2. A standard HNH seasonal cycle was calculated for the period between January 2004 and December 2007. After subtracting the overall Xco mean for 4 years of data, the obtained seasonal cycle (Table A2) was employed for deseasonalizing the measured Xco.
3. The data were also required to be detrended. The February-March points were chosen as the cold season with negligible biomass burning. The fifth-order polynomial for these points with the subtracted overall mean was obtained and assumed as the trend for the entire data set (Table A3)
4. The HNH box-averaged CO TC was subtracted by the trend and the seasonal cycle to represent the TC perturbed by fires. Then it was multiplied by the area of the HNH to obtain the monthly fire-induced total mass anomaly M'_{HNH} in Tg.
5. The anomaly was divided by 0.73 to correct for reduced sensitivity of measured CO (see Validation section above).

6. Loss terms in Equations (2) and (3) were calculated.
7. The wildfire emission P′ was calculated as a sum of the monthly changes in M'_{HNH} and two loss terms, transport into the LNH, L_{trans}, and loss of CO due to a reaction with hydroxyl (OH), L_{chem}; quotation marks indicate deviations from the 2004–2007 background (Equation (1)).

$$P' = M'_{HNH}/t + L_{trans} + L_{chem}, \quad (1)$$

$$L_{trans} = (M_{HNH} - M_{LNH})/\tau_{trans}, \quad (2)$$

$$L_{chem} = M'_{HNH}/\tau_{chem}, \quad (3)$$

$$CO + OH = CO_2 + H, \quad (4)$$

$$\tau_{chem} = 1/[OH] \cdot k, \quad (5)$$

$$k = 1.5 \cdot 10^{-13} (1 + 0.6 \cdot p)\ cm^3\ molec^{-1}\ s^{-1}, \quad (6)$$

where τ_{trans} was calculated using a 3-D GEOS-CHEM global CTM [10,16]. (OH) is the hydroxyl concentration [17] averaged over the HNH, k is the reaction (4) rate constant [18], and p is the air pressure in hPa. τ_{chem} varied between 1.4 and 27 months in July and December, respectively [10]. τ_{trans} and τ_{chem} are tabulated in Table A1.

2.4. Global Fire Emission Data

The end product of the GFED, version 4s [3] was a set of maps (0.25° · 0.25° latitude/longitude). The original approach was proposed in [2] and the GFED algorithm was improved several times afterwards. The CO emissions for latitude, longitude, and time t Eco were calculated as the sum of the emissions from various sources (savannah, boreal forest, peat, etc.):

$$Eco\ (lat, lon, t) = \Sigma\ EFco_{sources} \cdot DM\ (lat, lon, t) \cdot contrib_{sources}\ (lat, lon, t)$$

where $EFco_{sources}$ is the emission factor for CO (a fraction of dry matter DM); DM is a dry organic matter for (lat, lon, t), and $contrib_{sources}$ is the contribution of the various sources. The most important and critical parameter is the burned areas, which is obtained from the Moderate Resolution Imaging Spectroradiometer (MODIS) [4]. For our paper the Eco from the maps were summed over the HNH. Forest fires are found the primary driver of interannual variability in fire emissions [3].

3. Results

3.1. Xco Measured by AIRS

The maps of the spatial distribution of the Xco in August 2020 and 2021 (Figure 2) show a striking difference between the CO levels for these two consecutive years. Nevertheless, a common feature is the important role of boreal forest fires for CO variations. Note that CO from forest fires in 2021 spread to almost all the HNH, including the Arctic. August follows July, which is characterized by maximal emissions (see below). Therefore, one month is not enough for a significant transport of fire CO into tropical latitudes. It is noteworthy that the measurements of the HNH Xco everywhere, even far from the active fires, were important for the emissions estimates. It was necessary also to take into account the CO losses due to photochemical removal within the HNH and transport to southern latitudes.

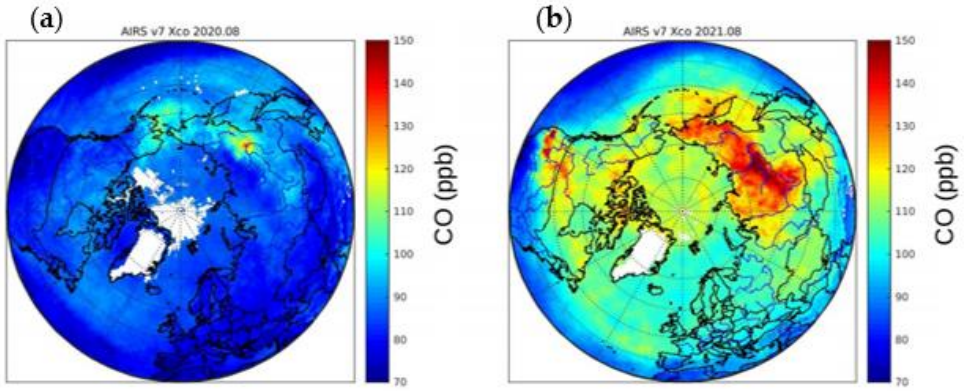

Figure 2. Monthly mean Xco for August 2020 (**a**) and August 2021 (**b**) measured by AIRS. Southern boundary of the maps is 30° N.

Figure 3 illustrates original measurements and modifications that are necessary to determine the fire effect on CO. Anthropogenic CO emission from automobiles, other kinds of transport as well as industry is a significant part of its global budget. Improvements in technology led to a long-term downward trend [11]. Seasonal variations for years with small wildfires experienced a maximum in March and a minimum in August [19]. They were determined mainly by the OH seasonal concentrations, which are minimal in dark/cold seasons. The maximum effect of biomass burning was observed in summer. The period of minimal summer disturbances (2004–2007) was taken to calculate the standard seasonal cycle. The original data were modified in an attempt to eliminate the trend and seasonal changes. The trend was defined as a fifth-degree polynomial for the February–March 2004–2022 data and applied to all the results. Therefore, the oscillating thin black line represents a "background". In other words, this line was taken as the Xco for no (or negligible) biomass burning emissions for all years. The difference ("*CO anomaly*") between the red line (measured Xco) and the thin black line (background) is displayed as green dots (right scale). This anomaly was considered the net effect of biomass burning. Verification efforts revealed an underestimation of about 30% of the measured anomaly. The CO anomaly was then corrected according to the validation results and used as input for the box model. Most striking is the record CO spike in July–August 2021. Also note the rapid increase in CO anomalies between June and August of each year and the subsequent gradual decrease due to photochemical and transport of extra CO to LNH with characteristic times of several months.

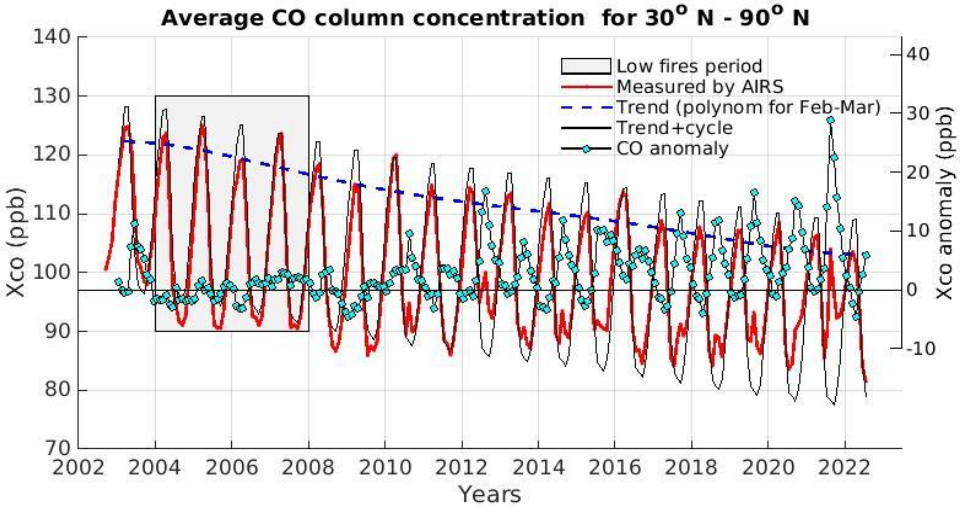

Figure 3. Original data, trend, seasonal cycle + trend (left scale), and fire-induced CO anomaly (right scale). Units are vertically averaged VMR in ppb.

3.2. Fire Emissions

Monthly HNH CO emissions from fires calculated using our box model are presented in Figure 4 as a function of time. Generally, maximum emissions occurred in July and sometimes in August. Months of maximum concentration (e.g., August 2021) usually followed months of maximum emissions (July 2021). Small negative emissions reflect the inaccuracies associated with the assumptions and/or other irregularities in CO emissions (e.g., the 2008–2009 economic downturn or the impact of the 2020–2021 COVID-19 pandemic).

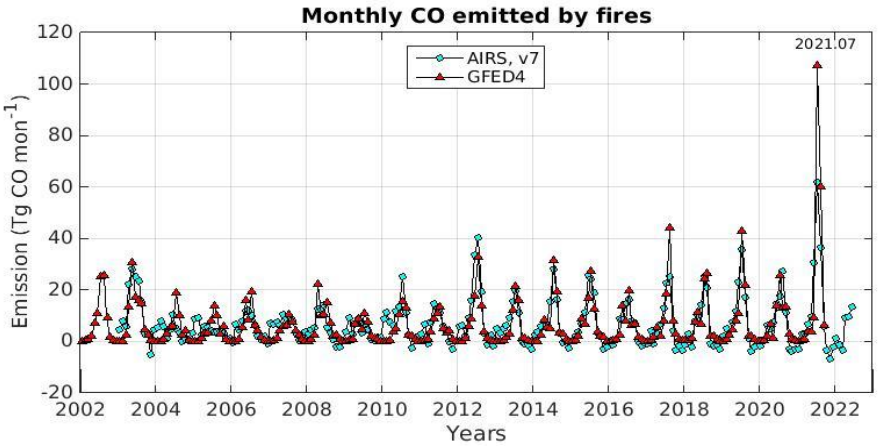

Figure 4. Monthly CO emissions from fires estimated from AIRS data and compared with GFED4c results [3] https://www.geo.vu.nl/~gwerf/GFED/GFED4c/.(accessed on 7 May 2022).

The GFED CO data were consistent with the AIRS data. The scatter plot (Figure 5) shows a clear correlation between the monthly emissions obtained by these two independent methods (slope 0.84 ± 0.07, 95% confidence interval, correlation coefficient R = 0.69). The monthly values of emissions differed by less than ~10 Tg/month in most data, and only the three circled summer points are scattered more. In all three cases, the AIRS data were lower than the emissions estimated by GFED4c. During these months (July and August), the most severe fires occurred. It is reasonable to assume that the additional CO was in the lower troposphere and the decrease in the sensitivity of the TIR instruments led to an underestimation. In order to confirm the remotely sensed data with more representativeness, ground control points are needed closer to the fire areas than the TCCON sites (see above).

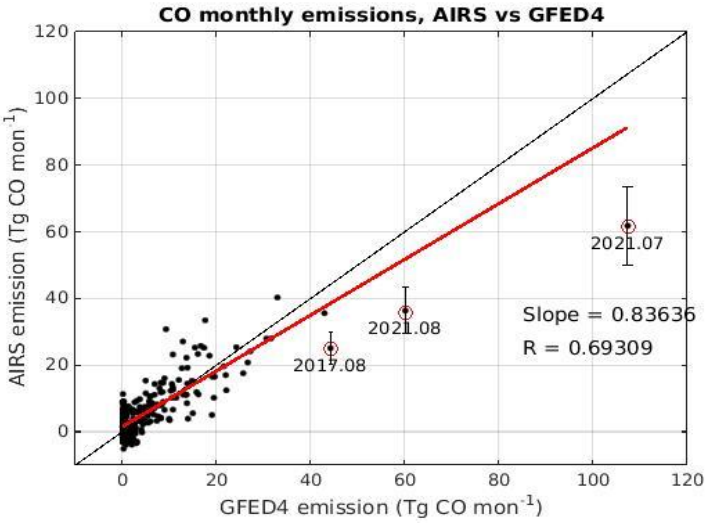

Figure 5. Monthly CO emitted by fires in HNH according to AIRS in comparison with GFED4c data [3]. Times for most scattered points are labeled. Error bars ± 19% here and in Figure 6 correspond to the accuracy of the correction for reduced sensitivity term.

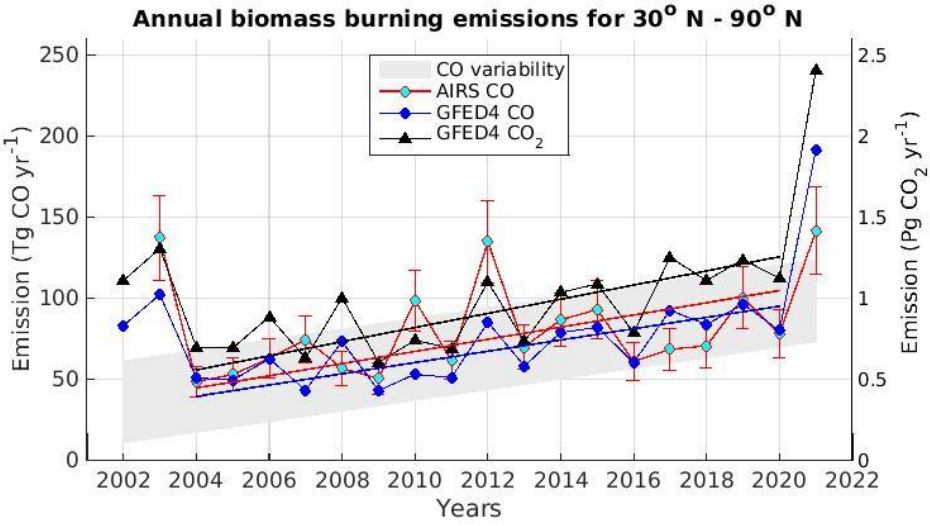

Figure 6. Annual CO emitted by fires in HNH according to AIRS data and bottom-up GFED4c estimates [3]. CO_2 emissions (right scale) [3] are plotted for comparison. Least-squares regression lines are also shown. Error bars are derived from the validation and are estimated as ±19%. The shaded area corresponds to GFED4c CO ± 2 STD (standard deviation) of the yearly points.

Annual CO emissions from AIRS and GFED4c are shown in Figure 6 and Table 2. The corresponding CO_2 emissions (for GFED4c only) are plotted in Figure 6 for comparison. After two years with severe fires in 2002 and 2003 [9], a relatively gradual increase in annual emissions was observed. The regression lines for 2004–2020 for AIRS (red) and GFED4c (blue) are almost parallel; the slopes are 3.6 ± 2.2 and 3.5 ± 1.3 Tg CO year^{-2}, respectively. The fire emissions of CO_2 increased at a rate of 43.6 ± 17 Tg CO_2 yr^{-2}. The relative trends were 4.8 ± 2.7, 5.1 ± 1.9, and 4.8 ± 1.9% yr^{-1} for AIRS CO, GFED4c CO, and GFED4c CO_2, respectively. Confidence intervals of 95% were obtained as described in [20]. The 2021 fires set a new record with AIRS detecting 89% more CO emissions compared to the 2004–2020 average. GFED4c estimated CO emission 182% more than in previous years.

Table 2. Annual HNH CO fire emissions in Tg yr^{-1} for this paper and from [9]. FTIR stands for Fourier transform infrared ground-based spectrometers.

Year	AIRS (This Paper)	GFED4c (This Paper)	FTIR [9]	MOPITT [9]
1998	-	114	151.4	
1999	-	48	32.3	
2000	-	50	−1.8	1.8
2001	-	43	5.1	−0.9
2002	-	83	120.6	118
2003	125	103	-	-
2004	49	51	-	-
2005	53	50	-	-
2006	63	63	-	-
2007	75	44	-	-
2008	57	74	-	-
2009	51	43	-	-
2010	99	53	-	-
2011	62	51	-	-
2012	135	85	-	-
2013	70	58	-	-
2014	87	79	-	-
2015	93	82	-	-
2016	61	61	-	-
2017	69	93	-	-
2018	71	84	-	-
2019	101	97	-	-
2020	78	80	-	-
2021	142	192	-	-

4. Discussion and Conclusions

The top-down MOPITT analysis [11] of the global and regional CO balance up to 2017 and specifically for wildfires in 2000–2019 [12] did not allow for making an unambiguous conclusion about the long-term trend of CO emissions from biomass combustion. For example, the absence of a statistically significant trend in the global CO wildfire emissions contradicted the decrease in the burned areas. Meanwhile, according to [12], "Canada and Alaska is the region where both burned areas and emission intensities increased rapidly, driving a substantial increase in its fire CO_2 emissions from the 2000s to the 2010s". The inverse global modeling used in these two studies is very complex. We believe that our simple box model based on AIRS data may help clarify this practical and scientifically important issue.

The point of accuracy is critical. A box model inversion of the July 2021 AIRS data (Figures 4 and 5) provided only half of the GFED4c estimates. The 2021 annualized GFED4c CO was also significantly higher than that of the AIRS data. This discrepancy did not appear to be a random fluctuation. We considered this underestimation to be the result of an unaccounted effect of the reduced sensitivity of AIRS CO to lower altitudes in the case of the strongest fire season. The validation was based on the ground truth sites that were far from the burning areas. Thus, an annual GFED4c emission of 195 Tg CO yr^{-1} appears to be closer to reality.

According to the estimates based on the box model analysis (Figure 6 and Table 2), the total CO emissions from biomass burning in the HNH were mostly in the range of 50–100 Tg CO yr^{-1}. For three years (2003, 2012, and 2021) wildfires emitted 125, 135, and 142 Tg CO yr^{-1}, respectively. A similar pattern of yearly CO emissions was found in the GFED4c database, except for 2012. After excluding the marginal values for 2003 and 2021, both approaches showed a statistically significant positive trend of 4.8–5.1 % yr^{-1}. The record high top-down and bottom-up emissions estimates for 2021 supported the finding of an increase in HNH biomass burning (mostly boreal fires) over the past decade. The possibility of further acceleration cannot be ruled out.

A 20-year data set (Figure 6) allowed us to propose a classification of fires depending on their intensity. All years with emissions within the shaded area can be considered years with *normal* fires. The fires of 2002, 2003, and 2021 can be classified as *catastrophic* (or *megafires*). Megafires happen from time to time and are likely due to long-lasting blockages in high-pressure systems (heat waves) and severe droughts. Such a classification can contribute to more reliable forecasting of the various types of forest fires.

Remote sensing satellite measurements combined with a box model allow rapid, almost immediate tracking of CO emissions from forest fires on a hemispheric or global scale. Despite several necessary simplifications, a comparison of the GFED4c bottom-up approach confirms the validity of our findings. A further improvement of this technique could be its combination with CTM: for example, a CTM may help to a better quantification of CO transport and photochemical sinks. Our model is not an alternative to comprehensive inverse modeling but is a means of the additional verification of the conclusions. This study focuses on the HNH as an important populated and industrialized area; forest fires can be a serious threat to it.

Author Contributions: Conceptualization, writing, validation, formal analysis, L.Y. Validation and data curation, V.R. All authors have read and agreed to the published version of the manuscript.

Funding: The study was funded in part by the Ministry of Science and Higher Education of the Russian Federation under agreement # 075-15-2020-776.

Institutional Review Board Statement: Not applicable.

Informed Consent Statement: Not applicable.

Data Availability Statement: AIRS datasets: https://disc.gsfc.nasa.gov/datasets/(accessed on 15 August 2022). GFED4c datasets: https://www.geo.vu.nl/~gwerf/GFED/GFED4c/(accessed on 7 May 2022). TCCON datasets: https://data.caltech.edu/records/20140 (accessed on 1 December 2021).

Acknowledgments: The authors express gratitude to Andrey Lapenis (the University of Albany, Albany, NY, USA) for his helpful discussions, to Guido van der Werf (Vrije Universiteit Amsterdam, Amsterdam, The Netherlands) for the detailed explanation of the GFED4c data set, and to Debra Wunch (University of Toronto, Toronto, ON, Canada) for guidance in using the TCCON validation data.

Conflicts of Interest: The authors declare no conflict of interest.

Appendix A

Table A1. Monthly mean characteristic times for air exchange between High and Low Northern Hemispheres τ_{trans} and photochemical lifetime τ_{chem}.

Month	τ_{trans} (Months)	τ_{chem} (Months)
1	1.7	23.8
2	2.1	14.0
3	3.5	6.5
4	3.4	3.4
5	2.1	2.1
6	1.5	1.4
7	1.5	1.4
8	1.6	1.8
9	2.4	3.5
10	2.6	7.3
11	2.8	15.8
12	1.5	27.2

Table A2. Seasonal cycle of Xco in HNH, calculated for the period January 2004–December 2007.

Month	Seasonal Cycle, ppb
1	8.0
2	13.5
3	17.5
4	17.7
5	7.1
6	−6.8
7	−12.6
8	−13.3
9	−14.0
10	−11.9
11	−6.1
12	0.9

Table A3. Trend (fifth-order polynomial) determined for the February-March period for all years and extrapolated onto the rest of the data; Xco (ppb).

Month/Year	2003	2004	2005	2006	2007	2008	2009	2010	2011	2012
1	10.4	10	9.1	7.7	6.2	4.7	3.3	2.1	1	0.1
2	10.4	10	9	7.6	6.1	4.6	3.2	2	0.9	0
3	10.4	9.9	8.9	7.5	5.9	4.4	3.1	1.9	0.8	−0.1
4	10.4	9.9	8.8	7.3	5.8	4.3	3	1.8	0.8	−0.1
5	10.3	9.8	8.6	7.2	5.7	4.2	2.9	1.7	0.7	−0.2
6	10.3	9.7	8.5	7.1	5.6	4.1	2.8	1.6	0.6	−0.3
7	10.3	9.6	8.4	7	5.4	4	2.7	1.5	0.5	−0.3
8	10.2	9.5	8.3	6.8	5.3	3.9	2.6	1.4	0.5	−0.4
9	10.2	9.4	8.2	6.7	5.2	3.8	2.5	1.4	0.4	−0.5
10	10.2	9.3	8.1	6.6	5.1	3.6	2.4	1.3	0.3	−0.5
11	10.1	9.2	7.9	6.4	4.9	3.5	2.3	1.2	0.2	−0.6
12	10.1	9.2	7.8	6.3	4.8	3.4	2.2	1.1	0.2	−0.7

Table A3. *Cont.*

Month/Year	2013	2014	2015	2016	2017	2018	2019	2020	2021
1	-0.8	−1.6	−2.4	−3.3	−4.2	−5.3	−6.4	−7.5	−8.3
2	−0.8	−1.6	−2.4	−3.3	−4.3	−5.4	−6.5	−7.6	−8.4
3	−0.9	−1.7	−2.5	−3.4	−4.4	−5.5	−6.6	−7.6	−8.4
4	−1	−1.8	−2.6	−3.5	−4.5	−5.6	−6.7	−7.7	−8.5
5	−1	−1.8	−2.7	−3.6	−4.6	−5.7	−6.8	−7.8	−8.5
6	−1.1	−1.9	−2.7	−3.7	−4.7	−5.8	−6.9	−7.8	−8.5
7	−1.2	−2	−2.8	−3.7	−4.8	−5.9	−6.9	−7.9	−8.6
8	−1.2	−2	−2.9	−3.8	−4.9	−5.9	−7	−8	−8.6
9	−1.3	−2.1	−3	−3.9	−4.9	−6	−7.1	−8	−8.6
10	−1.4	−2.2	−3	−4	−5	−6.1	−7.2	−8.1	−8.7
11	−1.4	−2.2	−3.1	−4.1	−5.1	−6.2	−7.3	−8.2	−8.7
12	−1.5	−2.3	−3.2	−4.2	−5.2	−6.3	−7.4	−8.3	−8.7

References

1. Kasischke, E.; Stocks, B. *Fire, Climate Change, and Carbon Cycling in the Boreal Forest*; Springer: New York, NY, USA, 2000; 461p.
2. Seiler, W.; Crutzen, P.J. Estimates of gross and net fluxes of carbon between the biosphere and the atmosphere from biomass burning. *Clim. Change* **1980**, *2*, 207–247. [CrossRef]
3. Van der Werf, G.R.; Randerson, J.T.; Giglio, L.; van Leeuwen, T.T.; Chen, Y.; Rogers, B.M.; Mu, M.; van Marle, M.J.E.; Morton, D.C.; Collatz, J.; et al. Global fire emissions estimates during 1997–2016. *Earth Syst. Sci. Data* **2017**, *9*, 697–720. [CrossRef]
4. Giglio, L.; Csiszar, I.; Justice, C.O. Global distribution and seasonality of active fires as observed with the Terra and Aqua Moderate Resolution Imaging Spectroradiometer (MODIS) sensors. *J. Geophys. Res. Biogeosci.* **2006**, *111*, G02016. [CrossRef]
5. Dekker, I.N.; Houweling, S.; Aben, I.; Röckmann, T.; Krol, M.; Martínez-Alonso, S.; Deeter, M.N.; Worden, H.M. Quantification of CO emissions from the city of Madrid using MOPITT satellite retrievals and WRF simulations. *Atmos. Chem. Phys.* **2017**, *17*, 14675–14694. [CrossRef]
6. Bela, M.M.; Kille, N.; McKeen, S.A.; Romero-Alvarez, J.; Ahmadov, R.; James, E.; Pereira, G.; Schmidt, C.; Pierce, R.B.; O'Neill, S.M.; et al. Quantifying carbon monoxide emissions on the scale of large wildfires. *Geophys. Res. Lett.* **2021**, *49*, e2021GL095831. [CrossRef]
7. Deeter, M.; Francis, G.; Gille, J.; Mao, D.; Martínez-Alonso, S.; Worden, H.; McKain, K. The MOPITT Version 9 CO product: Sampling enhancements and validation. *Atmosph. Meas. Tech.* **2022**, *15*, 2325–2344. [CrossRef]
8. Aumann, H.H.; Chahine, M.T.; Gautier, C.; Goldberg, M.D.; Kalnay, E.; McMillin, L.M.; Revercomb, H.P.; Rosenkranz, P.W.; Smith, W.L.; Staelin, D.H.; et al. AIRS/AMSU/HSB on the Aqua mission: Design, science objectives, data products and processing systems. *IEEE Trans. Geosci. Rem. Sens.* **2003**, *41*, 253–264. [CrossRef]
9. Yurganov, L.N.; Duchatelet, P.; Dzhola, A.V.; Edwards, D.P.; Hase, F.; Kramer, I.; Mahieu, E.; Mellqvist, J.; Notholt, J.; Novelli, P.C.; et al. Increased Northern Hemispheric carbon monoxide burden in the troposphere in 2002 and 2003 detected from the ground and from space. *Atmos. Chem. Phys.* **2005**, *5*, 563–573. [CrossRef]
10. Yurganov, L.N.; Blumenstock, T.; Grechko, E.I.; Hase, F.; Hyer, E.J.; Kasischke, E.S.; Koike, M.; Kondo, Y.; Kramer, I.; Le-ung, F.-Y.; et al. A quantitative assessment of the 1998 carbon monoxide emission anomaly in the northern Hemisphere based on total column and surface concentration measurements. *J. Geophys. Res.* **2004**, *109*, D15305. [CrossRef]
11. Zheng, B.; Chevallier, F.; Yin, Y.; Ciais, P.; Fortems-Cheiney, A.; Deeter, M.N.; Parker, R.J.; Wang, Y.; Worden, H.M.; Zhao, Y. Global atmospheric carbon monoxide budget 2000-2017 inferred from multi-species atmospheric inversions. *Earth Syst. Sci. Data* **2019**, *11*, 1411–1436. [CrossRef]
12. Zheng, B.; Ciais, P.; Chevallier, A.; Chuvieco, E.; Chen, Y.; Yang, H. Increasing forest fire emissions despite the decline in global burned area. *Sci. Adv.* **2021**, *7*, eabh2646. [CrossRef] [PubMed]
13. Tian, B.; Manning, R.J.; Thrastarson, H.; Fetzer, E.; Monarrez, R. AIRS Version 7 Level 3 Product User Guide. 2020. Available online: https://docserver.gesdisc.eosdis.nasa.gov/public/project/AIRS/V7_L3_User_Guide.pdf (accessed on 18 August 2022).
14. Wunch, D.; Toon, G.C.; Blavier, J.-F.L.; Washenfelder, R.A.; Notholt, J.; Connor, B.J.; Griffith, D.W.T.; Sherlock, V.; Wennberg, P.O. The Total Carbon Column Observing Network. *Philos. Trans. R. Soc. A Math. Phys. Eng. Sci.* **2011**, *369*, 2087–2112. [CrossRef] [PubMed]
15. Rakitin, V.S.; Elansky, N.F.; Skorokhod, A.I.; Dzhola, A.V.; Rakitina, A.V.; Shilkin, A.V.; Kirillova, N.S.; Kazakov, A.V. Long-Term Tendencies of Carbon Monoxide in the Atmosphere of the Moscow Megapolis. *Izv. Atmos. Ocean Phys.* **2021**, *57*, 116–125. [CrossRef]
16. Holloway, T.; Levy, H., II; Kasibhatla, P. Global distribution of carbon monoxide. *J. Geophys. Res.* **2000**, *105*, 12123–12147. [CrossRef]
17. Spivakovsky, C.M.; Logan, J.A.; Montzka, S.A.; Balkanski, Y.J.; Foreman-Fowler, M.; Jones, D.B.A.; Horowitz, L.W.; Fusco, A.C.; Brenninkmeijer, C.A.M.; Prather, M.J.; et al. Three-dimensional climatological distribution of tropospheric OH: Update and evaluation. *J. Geophys. Res.* **2000**, *105*, 8931–8980. [CrossRef]

18. DeMore, W.B.; Sander, S.P.; Golden, D.M.; Hampson, R.F.; Kurylo, M.J.; Howard, C.J.; Ravishankara, A.R.; Kolb, C.E.; Molina, M.J. Chemical kinetics and photochemical data for use in stratospheric modeling. *JPL Publ.* **1997**, *3*, 94–97.
19. Dianov-Klokov, V.I.; Yurganov, L.N. A spectroscopic study of the global space-time distribution of atmospheric CO. *Tellus* **1981**, *33*, 262–273. [CrossRef]
20. Chatterjee, S.; Hadi, A.S. Influential observations, high leverage points, and outliers in linear regression. *Stat. Sci.* **1986**, *1*, 379–416.